



CHORUS

This is the accepted manuscript made available via CHORUS. The article has been published as:

Velocity plateaus in traveling-wave electrophoresis

Robert Correll and Boyd F. Edwards

Phys. Rev. E **86**, 041916 — Published 25 October 2012

DOI: [10.1103/PhysRevE.86.041916](https://doi.org/10.1103/PhysRevE.86.041916)

Velocity plateaus in traveling-wave electrophoresis

Robert Correll
Department of Physics
West Virginia University
Morgantown, WV 26506

Boyd F. Edwards
Department of Physics
Utah State University Uintah Basin
Vernal, Utah 84078
 (Dated: September 20, 2012)

One-dimensional models are used to study traveling wave electrophoresis, a tunable method for separating charged analytes. A traveling-electrode model reveals the mechanism for longitudinal oscillations. A stationary-electrode model explains the origin of mode-locked plateaus in the average velocity, predicts devil's staircases with nested Farey sequences, and reduces to a continuum sinusoidal model in the high electrode-density limit.

PACS numbers: 87.50.C-, 82.45.-h, 87.50.ch

One of the goals of microfluidics is to develop robust inexpensive methods of separating analytes on lab-on-a-chip devices. Such methods might be useful in a wide variety of applications [1]. Traveling wave electrophoresis is a separation method that has been investigated recently [2–5]: four interdigitated electrode arrays alternate along a channel as shown in Fig. 1. These arrays are held at four AC potentials $\Phi_0(t)$, $\Phi_1(t)$, $\Phi_2(t)$, and $\Phi_3(t)$ of the same amplitude ϕ_0 and frequency ω , but with adjacent potentials differing in phase by 90° . These potentials create an electric potential wave that travels along the axis of the channel, with a four-electrode pattern of wavelength λ replicated indefinitely along the channel, of height h . This wave traps high-mobility analyte particles, carrying them along the channel at an average velocity equal to the wave speed. The wave partially traps intermediate-mobility particles that move at an average velocity that is less than the wave speed. The wave confines low-mobility particles to the vicinity of electrodes, resulting in zero average velocity.

The dynamics are governed by the dimensionless mobility,

$$R = \frac{\mu E_0}{c}, \quad (1)$$

involving the electrophoretic mobility μ , the electric field amplitude $E_0 = k\phi_0$, the wave speed $c = \omega/k$, and the wave number $k = 2\pi/\lambda$.

A numerical single-particle model of transport through the two-dimensional (2D) channel of Fig. 1B exhibits plateaus in the average dimensionless particle velocity u/c (Fig. 2, for channel aspect ratio $\lambda/h = 4$ [2]). Single-particle models pertain to dilute systems in which electrode screening can be ignored. For low mobilities $R < R_l$, particles are confined to the locality of electrodes and $u = 0$. For high mobilities $R > R_t$, particles are trapped by the wave and $u = c$. As R increases from the localization threshold R_l to the trapping threshold

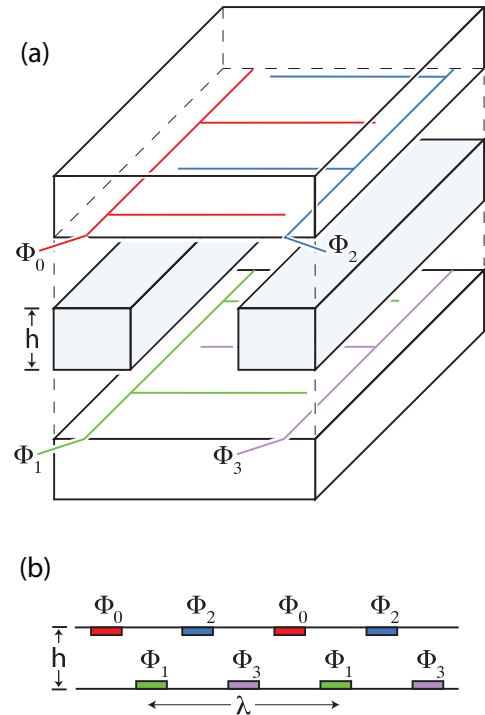


FIG. 1: Exploded view (a) and side view (b) of the geometry of the experimental traveling-wave electrophoresis device [2–5], with channel height h and four electrodes per wavelength, λ . These electrodes are held at the AC potentials $\Phi_0(t)$, $\Phi_1(t)$, $\Phi_2(t)$, and $\Phi_3(t)$, each potential differing in phase by 90° from its neighbor to the left.

R_t , u generally rises from zero to c , but not monotonically. Of particular interest are the plateaus at $u/c = 1/9$ and $u/c = 1/5$ where the average velocity remains at a constant finite rational fraction of the wave speed over a range of mobilities.

The purpose of this paper is to investigate the physical

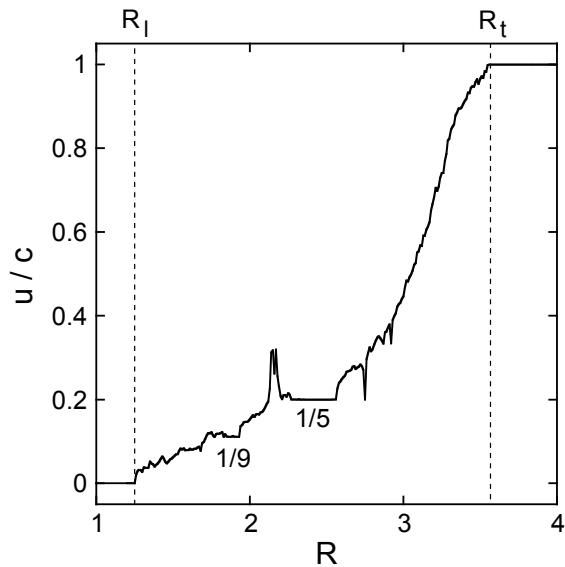


FIG. 2: Simulated average dimensionless particle velocity u/c vs. dimensionless mobility R for the 2D geometry of Fig. 1(b) with wavelength to height ratio $\lambda/h = 4$ [2]. Within velocity plateaus at $u/c = 1/5$ and $1/9$, u/c is independent of R . Labeled are the localization and trapping thresholds $R_l = 1.26$ and $R_t = 3.56$.

origin of these plateaus using 1D single-particle models of traveling-wave electrophoresis. We review the sinusoidal model that has been studied previously [2, 6, 7], introduce traveling-electrode and stationary-electrode models, and show that only the stationary-electrode model produces plateaus. Experiments [3–5] have observed localization and trapping thresholds as predicted by the 2D model [2, 3], but have not yet observed velocity plateaus. These plateaus might just be observable in careful experiments, but their physical origin is unclear. Better understanding of these plateaus may help to guide the development of future experiments designed to improve microfluidic separation techniques.

I. 1D SINUSOIDAL MODEL

We first consider a simple 1D model of a longitudinal sine wave traveling in the $+x$ direction, with electric potential

$$\phi(x, t) = \phi_0 \sin(kx - \omega t). \quad (2)$$

This model ignores the discreteness of the electrodes and collapses the system to one dimension. Writing the longitudinal electric field as $E_x(x, t) = -\partial\phi/\partial x$ and solving

$$\dot{x} = \mu E_x(x, t) \quad (3)$$

for the particle position $x(t)$ yields, after the decay of transients, regular longitudinal oscillations for $|R| < 1$

and a constant trapped velocity $u = c$ for $|R| \geq 1$, with a time average velocity $u = \langle \dot{x} \rangle$ satisfying [2, 6]

$$\frac{u}{c} = \begin{cases} 1 - (1 - R^2)^{1/2}, & |R| < 1 \\ 1, & |R| \geq 1 \end{cases}. \quad (4)$$

This average velocity increases monotonically with increasing $|R|$ up to the trapping threshold $R_t = 1$, beyond which the particle is fully trapped by the wave. This model evidently gives no localization threshold and no velocity plateaus.

II. 1D TRAVELING-ELECTRODE MODEL

The simplest model with discrete electrodes is to represent each wavelength of the traveling wave by a pair of electrodes that are separated by a distance of $\lambda/2$, that are held at fixed electrical potentials $\phi = \pm\phi_0$, and that are moving with speed c .

One way to realize this model experimentally is to use a moving lattice of planar conducting screens (wire meshes) spaced half a wavelength apart, with screens maintained at fixed potentials that alternate between $\phi = +\phi_0$ and $\phi = -\phi_0$ as one moves from one screen to the next. The lattice moves through an otherwise stationary fluid at a uniform velocity of magnitude c directed perpendicular to the planes of the screens, with fluid streaming through the gaps in the screens.

Between the electrodes, the solution is assumed to be electroneutral and is therefore governed by the Laplace equation,

$$\frac{d^2\phi}{dx^2} = 0, \quad (5)$$

yielding a traveling triangle-wave potential of amplitude ϕ_0 and wavelength λ , and a corresponding traveling longitudinal square-wave electric field $\mathbf{E} = -\hat{x}\partial\phi/\partial x$ of amplitude $E_0 = 4\phi_0/\lambda$. (This relationship applies only to the 1D traveling-electrode model; the relationship $E_0 = k\phi_0$ applies elsewhere in this paper.) This square wave alternates between the fixed values $\mathbf{E} = \pm E_0\hat{x}$ every half wavelength, and propagates at speed c in the $+x$ direction.

A positively charged particle (with $\mu > 0$ and $R > 0$) in this field has constant speed $v_0 = \mu E_0$ in the $+x$ direction (in the direction of the wave) in peaks of the square wave where $\mathbf{E} = +E_0\hat{x}$, and has constant speed v_0 in the $-x$ direction (opposite to the wave) in valleys where $\mathbf{E} = -E_0\hat{x}$.

For $0 < R < 1$, noting that $R = v_0/c$ from Eq. (1), the particle speed v_0 is less than the wave speed c , and positively charged particles in peaks of the wave fall short of keeping pace with the wave. In the frame moving with the wave, such particles move in the $-x$ direction, at relative speed $c - v_0$ in peaks and at larger relative speed $c + v_0$ in valleys. Since each peak and each valley in the (square) wave has width $\lambda/2$, such particles

spend time $\Delta t_+ = \lambda/2(c - v_0)$ in peaks and less time $\Delta t_- = \lambda/2(c + v_0)$ in valleys, where particles more quickly cross the distance $\lambda/2$. In the laboratory frame, the particle undergoes longitudinal oscillations during which it moves at velocity $\mathbf{v} = +v_0\hat{x}$ for a time Δt_+ and for a positive displacement $\Delta x_+ = v_0\Delta t_+$, then moves at velocity $\mathbf{v} = -v_0\hat{x}$ for a shorter time Δt_- and for a shorter negative displacement $\Delta x_- = -v_0\Delta t_-$. The longitudinal oscillation cycle therefore has period $\Delta t_+ + \Delta t_-$, angular frequency

$$\Omega = \frac{2\pi}{\Delta t_+ + \Delta t_-} = 2\pi \frac{c^2 - v_0^2}{\lambda c}, \quad (6)$$

and net positive displacement $\Delta x_+ + \Delta x_-$. Accordingly, during longitudinal oscillations, the particle moves in the $+x$ direction with average speed

$$u = \frac{\Delta x_+ + \Delta x_-}{\Delta t_+ + \Delta t_-} = v_0^2/c. \quad (7)$$

The motion is similar to that of an inexperienced surfer who, unable to keep pace with each passing wave and occasionally lagging behind a wave, spends more time on the front sides of the waves (which push him forward, toward shore) than the back sides. In this way, the surfer makes net progress toward the shore. The more proficient the surfer, the closer his swimming speed v_0 comes to the wave speed c and the smaller his lag frequency Ω .

For $R > 1$, the particle speed $v_0 > c$ exceeds the wave speed, and, after a short transient, positively charged particles equilibrate at the leading edge of peaks in the wave, where the field drops from $+E_0$ (in peaks) to $-E_0$ (in valleys). Particles therefore maintain a constant speed

$$u = c \quad (8)$$

at this stable leading edge. A particle that lags slightly behind this leading edge will quickly catch up to the leading edge, whereas a particle that moves ahead of the leading edge into the adjacent valley will quickly return to the leading edge. This leading edge in the square electric-field wave corresponds to a minimum in the triangular potential wave.

Negatively charged particles with $\mu < 0$ and $R < 0$ behave similarly. For $|R| < 1$, such particles exhibit longitudinal oscillations with frequency Ω given by Eq. (6) and average velocity u in the $+x$ direction given by Eq. (7). The difference is that such particles spend more time in valleys, where in the laboratory frame they move with speed v_0 in the $+x$ direction, than in peaks, where they move with speed v_0 in the opposite direction. The oscillation frequencies and average velocities of negatively and positively charged particles are the same because their net displacements during each oscillation are the same. For $|R| > 1$, negatively charged particles equilibrate at the leading edges of valleys in the electric-field wave (and at peaks in the potential wave), where they travel with constant speed $u = c$.

In summary, the 1D traveling-electrode model gives an average particle velocity satisfying

$$\frac{u}{c} = \begin{cases} R^2, & |R| < 1 \\ 1, & |R| \geq 1 \end{cases} \quad (9)$$

and a longitudinal oscillation frequency satisfying

$$\frac{\Omega}{\omega} = \begin{cases} 1 - R^2, & |R| < 1 \\ 0, & |R| \geq 1 \end{cases}, \quad (10)$$

pertinent to both positively and negatively charged particles, where $\omega = ck$ is the angular frequency of the wave.

The traveling-electrode model reveals longitudinal oscillations to be the result of consecutive failed attempts by the particle to “catch” a passing wave, with the particle spending more time on the front sides of waves than the back sides and thereby making net forward progress in the direction of the wave. Similar oscillations are also seen in 2D simulations and in the 1D stationary electrode model. As is evident from Eq. (9), discrete traveling electrodes held at constant potentials produce no localization threshold and no velocity plateaus.

III. 1D STATIONARY-ELECTRODE MODEL

A third 1D alternative, which better replicates the actual experimental device, is to use discrete electrodes that are fixed in space but whose potentials oscillate with time. This model can be realized physically by using conducting screens that are fixed in space, and through which particles can pass, after the manner of the 1D traveling-electrode model. For N electrodes per wavelength located at positions $x_n = \lambda n/N$, with integer n , we apply to Eq. (2) for the time-dependent potential of electrode n ,

$$\Phi_n(t) = \phi_0 \sin(2\pi n/N - \omega t), \quad (11)$$

Electroneutrality is assumed between the electrodes, whence Eq. (5) ensures a potential $\phi(x, t)$ that is continuous and piecewise linear between electrodes, as illustrated for $N = 4$ in Figure 3. This potential changes shape as it propagates in the $+x$ direction, in contrast with the sinusoidal and traveling-electrode models whose potentials maintain constant shapes in the frame moving with the wave. Accordingly, the x -component of the electric field $E_n(t)$ between electrode n and electrode $n + 1$ is spatially uniform and depends on time according to

$$E_n(t) = -\frac{\Phi_{n+1}(t) - \Phi_n(t)}{\lambda/N}. \quad (12)$$

A convenient dimensionless equation of motion,

$$\frac{dx'}{dt'} = R \frac{N}{\pi} \sin \frac{\pi}{N} \sin \left[\frac{2\pi}{N} (t' - [x']) \right], \quad (13)$$

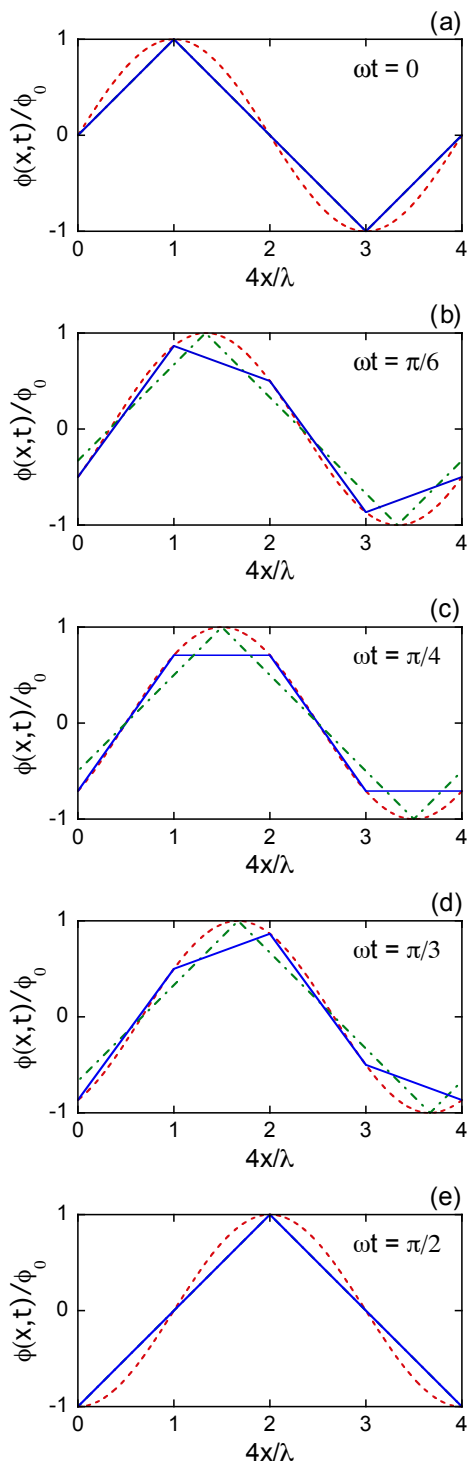


FIG. 3: Comparison of periodic 1D potentials for the sinusoidal (dashed), traveling-electrode (chain), and stationary-electrode (solid) models at times given by $\omega t = 0, \pi/6, \pi/4, \pi/3$, and $\pi/2$ (a, b, c, d, and e). Four stationary electrodes per wavelength ($N = 4$) are located at $4x/\lambda = 0, 1, 2, 3$, and 4 (solid), while traveling electrodes are located at the moving peaks and valleys of the triangle wave (chain). When traveling electrodes coincide with stationary electrodes, the traveling-electrode and stationary-electrode models give the same instantaneous potential (a and e).

follows from Eqs. (1), (3), (11), and (12). Here,

$$x' = \frac{x}{\lambda/N} \quad (14)$$

is a dimensionless position measured in units of the electrode spacing λ/N and

$$t' = \frac{t}{\tau/N} - \frac{1}{2} - \frac{N}{4} \quad (15)$$

is a dimensionless time measured in units of τ/N , where $\tau = 2\pi/\omega$ is the wave period. In this way, N represents both the dimensionless wavelength and the dimensionless period, and a particle that is trapped by the wave has average dimensionless velocity $u/c = \Delta x'/\Delta t' = 1$. The floor function $\lfloor x' \rfloor$ is the largest integer that is less than or equal to x' , and specifies the electrode number at or immediately to the left of the current position x' of the particle, with $\lfloor x' \rfloor \leq x'$. Equation (13) is readily integrated piecewise to find $x'(t')$ explicitly.

The stationary electrode model exhibits intriguing behavior including localization thresholds and velocity plateaus that are absent from the other 1D models. Figure 4 shows plots of $x'(t')$ for $N = 4$ and various values of R . For positively charged particles with $R > 0$, Eq. (13) demands $dx'/dt' > 0$ in shaded regions and $dx'/dt' < 0$ in unshaded regions. Hence, trapped positively charged particles travel in shaded regions. Trapped negatively-charged particles with $R < 0$ travel in unshaded regions, where $dx'/dt' > 0$ for these particles. Trace 0 shows a low-mobility, localized particle that oscillates about a single electrode, failing each attempt to progress to the next electrode. Such localized modes also occur in the 2D model [2]. Traces 1-8 show particles with successively larger mobilities executing longitudinal oscillations; these particles move along with the wave until they fall behind and return to the last electrode to await the next opportunity to move forward again. Trace ∞ shows a trapped high-mobility particle that moves successfully from electrode to electrode with an average speed equal to the wave speed.

For trace 0 in Fig. 4, the oscillation cycle lasts four quarter periods and the particle oscillates about the electrode located at $x' = 0$, never reaching the $x' = 1$ electrode and experiencing no net displacement ($\Delta x' = 0$). Thus, the particle is localized and has average velocity $u = 0$.

For trace 1 in Fig. 4, the particle is partially trapped by the wave. The oscillation cycle lasts five quarter periods ($\Delta t' = 5$) during which the particle moves forward by one electrode ($\Delta x' = 1$), giving average dimensionless velocity $u/c = \Delta x'/\Delta t' = 1/5$. For $0 < t' < 3$, the particle is carried forward by the wave, while for $3 < t' < 4.4$, the particle is pushed back by the passing wave in a manner reminiscent of the behavior of the 1D sinusoidal and traveling-electrode models. For $4.4 < t' < 5$, the particle remains fixed at electrode $x' = 1$, a stable potential minimum. Such stationary behavior is absent from the other 1D models but is present in the 2D model.

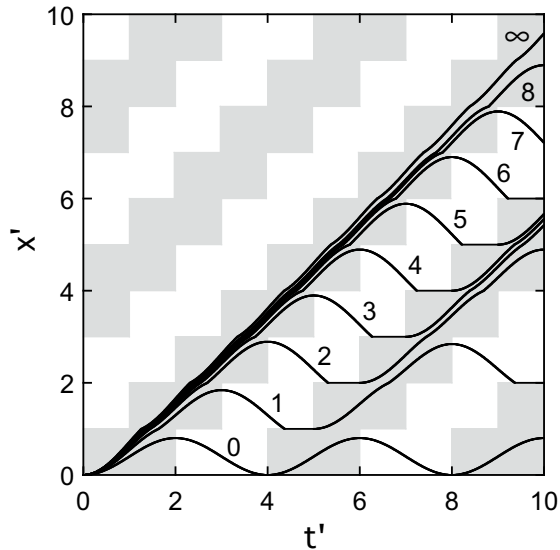


FIG. 4: Dimensionless particle displacements x' vs. dimensionless time t' for the 1D stationary-electrode model, with $N = 4$ electrodes per wavelength. The displacement is measured in units of a quarter wavelength and the time measured in units of a quarter period. Traces for dimensionless mobilities $R = 0.7, 0.95, 1.06, 1.11, 1.14, 1.16, 1.175, 1.185, 1.193,$ and 1.25 are labeled respectively by integers $\Delta x' = 0, 1, 2, 3, 4, 5, 6, 7, 8, \infty$ representing the displacement during each longitudinal oscillation cycle, where the $\Delta x' = 0$ trace represents a localized particle and the $\Delta x' = \infty$ trace represents a trapped particle. Velocities satisfy $dx'/dt' > 0$ in shaded regions and $dx'/dt' < 0$ in unshaded regions, according to Eq. (13) for $R > 0$.

Stationary behavior occurs when a positively-charged particle finds itself in a stable potential minimum, such as the minimum in the 1D stationary-electrode potential at electrode 3 in frames (a) and (b) of Fig. 3. Once such a particle reaches such a stable potential minimum, the particle cannot leave the electrode until it becomes unstable, as seen in frame (c), when the minimum shifts instantaneously from electrode 3 to electrode 4. Particles arriving at different times at a stable electrode all remain at that electrode until it becomes unstable. Negatively-charged particles are stable at maxima in the potential.

A positively charged particle that arrives at $x' = 0$ at a time satisfying $-1 < t' < 0$ will remain at $x' = 0$ until $t' = 0$, when the $x' = 0$ electrode becomes unstable and the particle is released from that electrode. Particles with different values of x' at $t' = 0$ eventually find their way to a stable electrode, where they remain until that electrode becomes unstable, and the subsequent behavior is identical to the behavior shown in Fig. 4 (apart from an offset in t' and x'). Thus, transient behavior ends as soon as a particle arrives at a stable electrode.

This stationary behavior is responsible for velocity plateaus and mode locking illustrated in Fig. 5. For example, all particles with mobilities $0.87 < R < 1.02$ that depart from electrode $x' = 0$ at time $t' = 0$ arrive at

electrode $x' = 1$ at different times $t' > 4$, but all depart from that electrode when it becomes unstable, at $t' = 5$. Consequently, all particles in this range, including trace 1 for $R = 0.95$ shown in Fig. 4, are locked into the same mode and have the same average velocity, $u/c = 1/5$, and the same oscillation frequency, $\Omega/\omega = N/t' = 4/5$. Thus, the $u/c = 1/5$ velocity plateau in Fig. 5 has the mobility range $0.87 < R < 1.02$. The longitudinal oscillation frequency decreases with increasing R as for the traveling-electrode model [see Eq. (10)], but is restricted to rational fractions.

In contrast to the other 1D models, for which potential minima travel at a constant speed equal to the wave speed, the stationary-electrode model features potential minima and maxima that remain at fixed positions in space until such time as the changing electrode potentials cause extrema to move instantaneously from electrode to electrode. The average velocity of the motion of these extrema equals the wave speed. Although potential extrema move instantaneously from electrode to electrode, particles take a finite time to travel from electrode to electrode in response to the potential. The 2D models and the experiments depicted in Fig. 1 behave likewise.

When a potential minimum jumps from one electrode to the next, a positively charged particle located at the first electrode begins an attempt to reach the second. The success of the particle in reaching the second electrode rests on the particle mobility. A high-mobility particle quickly covers the distance λ/N between the electrodes, reaching the second electrode before a time τ/N has elapsed, this being the time during which the potential minimum remains at each electrode. Such high-mobility particles keep pace with, and are trapped by, the wave. A low-mobility particle fails to cover the distance in this amount of time, and faces the possibility of being driven back to the first electrode.

Also shown in Fig. 5 are localization and trapping thresholds R_l and R_t that can be calculated explicitly. The localization threshold R_l represents the maximum value of $|R|$ for which the particle makes no net forward progress; the particle simply oscillates about a particular electrode, as shown for the localized particle in Fig. 4. To calculate the localization threshold, we note that a particle that fails to reach the next electrode in half a period $N/2$, when the velocity turns negative, will never reach that electrode. We accordingly integrate Eq. (13) from the initial position $x' = 0$ at time $t' = 0$ (after the decay of transients) to the final position $x' = 1$ at time $t' = N/2$, yielding

$$R_l = \frac{\pi^2/N^2}{\sin(\pi/N)}. \quad (16)$$

A particle with $|R| < R_l$ will never reach the next electrode. This result agrees with our solutions of Eq. (13) for various values of N , which show localization for $|R| \leq R_l$. This result also reduces to the 1D sinusoidal model result $R_l = 0$ for $N \rightarrow \infty$. For $N = 4$, $R_l = \sqrt{2}\pi^2/16 = 0.87$ (Fig. 5).

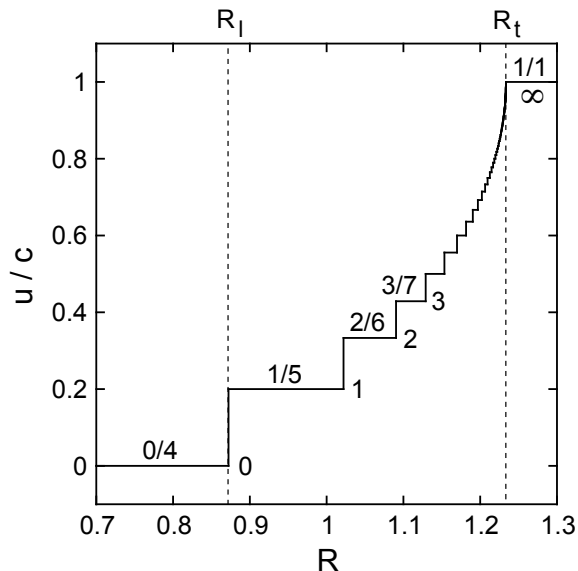


FIG. 5: Average dimensionless particle velocities u/c for the 1D stationary-electrode model with $N = 4$ electrodes per wavelength vs. the dimensionless mobility R . Shown are localization and trapping thresholds $R_l = \sqrt{2}\pi^2/16 = 0.87$ and $R_t = \pi^2/8 = 1.23$ from Eqs. (16) and (18). In the body of the plot, rational fractions represent values of u/c given by the $0/4 \rightarrow 1/1$ Farey sequence [Eqs. (19)-(24)], and isolated integers represent values of the sequence index m . These values coincide in this case with displacements $\Delta x'$ during longitudinal oscillations (Fig. 4). Each trace in Fig. 4 belongs to a different velocity plateau in Fig. 5.

To calculate R_t , we observe that, after the decay of transients, trapped particles travel a distance $\Delta x' = 1$ in a time $\Delta t' = 1$, as shown for the trapped particle in Fig. 4. We integrate Eq. (13) from the initial position $x' = 0$ at time $t' = t^*$ to the final position $x' = 1$ at time $t' = t^* + 1$, yielding

$$\cos \left[\frac{2\pi}{N} (t^* + 1) \right] = \cos \left(\frac{2\pi t^*}{N} \right) - \frac{2\pi^2/N^2}{R \sin(\pi/N)}, \quad (17)$$

which gives the electrode crossing time t^* as a function of R and N . The trapping threshold R_t is the minimum value of $|R|$ that admits a solution from Eq. (17). Differentiating this equation with respect to t^* , holding N constant, and setting $dR/dt^* = 0$ gives the crossing time $t^* = N/4 - 1/2$ at the trapping threshold for positively charged particles with $R > 0$, and $t^* = 3N/4 - 1/2$ for negatively charged particles with $R < 0$. Substituting these times into Eq. (17) gives the trapping threshold,

$$R_t = \frac{\pi^2/N^2}{\sin^2(\pi/N)}. \quad (18)$$

This result agrees with our solutions of Eq. (13) for various values of N , which show trapping for $|R| \geq R_t$. This result also reduces to the 1D sinusoidal model result $R_t = 1$ for $N \rightarrow \infty$. For $N = 4$, $R_t = \pi^2/8 = 1.23$ (Fig. 5).

Between R_l and R_t in Fig. 5, the velocity u/c ascends a staircase of decreasing step sizes, with steps at

$$\frac{u_m}{c} = \frac{m}{4+m}, \quad (19)$$

where $m = 0, 1, 2, \dots, \infty$.

Equation (19) is an example of an $a/b \rightarrow c/d$ Farey sequence, defined for integers a, b, c , and d as the sequence of rational fractions

$$\frac{a+mc}{b+md}, \quad (20)$$

for $m = 0, 1, 2, \dots, \infty$. This sequence begins at a/b for $m = 0$ and ends at c/d for $m \rightarrow \infty$. Thus Eq. (19) is a $0/4 \rightarrow 1/1$ Farey sequence.

The successive values of u_m/c shown in Fig. 5 can be obtained either from Eq. (19) or by Farey addition, defined as [8]

$$\frac{a}{b} \oplus \frac{c}{d} = \frac{a+c}{b+d}. \quad (21)$$

The $m = 1, 2$, and 3 iterates are

$$\frac{0}{4} \oplus \frac{1}{1} = \frac{1}{5} \quad (22)$$

$$\frac{1}{5} \oplus \frac{1}{1} = \frac{2}{6} \quad (23)$$

$$\frac{2}{6} \oplus \frac{1}{1} = \frac{3}{7}. \quad (24)$$

Because Farey addition of two fractions is accomplished by summing their numerators and their denominators without finding a common denominator, reduction of fractions is not permissible. For example, replacing $2/6$ by $1/3$ in Eq. (24) gives $2/4$ for the $m = 3$ velocity instead of the correct result of $3/7$.

In summary, the average dimensionless velocity u/c for the 1D stationary-electrode model with $N = 4$ electrodes is a piecewise constant function with values of the dimensionless velocity u/c given by the $0/4 \rightarrow 1/1$ Farey sequence (Fig. 5).

Increasing the electrode density yields richer behaviors. For $N = 8$, the salient features are given by the $0/8 \rightarrow 1/1$ Farey sequence (Fig. 6), but other structures are clearly present. Figure 7 reveals a Farey sub-sequence between the $0/8$ and $1/9$ plateaus. Figure 8(a) reveals a sub-sequence between the $2/10$ and $3/11$ plateaus and Fig. 8(b) reveals a $2/10 \rightarrow 5/21$ sub-sub-sequence within the $2/10 \rightarrow 3/11$ sub-sequence. Figure 9(a,b) shows an ascending $4/12 \rightarrow 5/13$ sub-sequence (a) and a descending $4/12 \leftarrow 5/13$ sub-sequence (b) over the same interval. Fig. 9(c) shows the ascending and descending sub-sub-sequences $9/25 \rightleftharpoons 14/38$, and hints at yet further detail. With each step in the $0/8 \rightarrow 1/1$ sequence containing an infinite number of sub-steps, and with many sub-steps

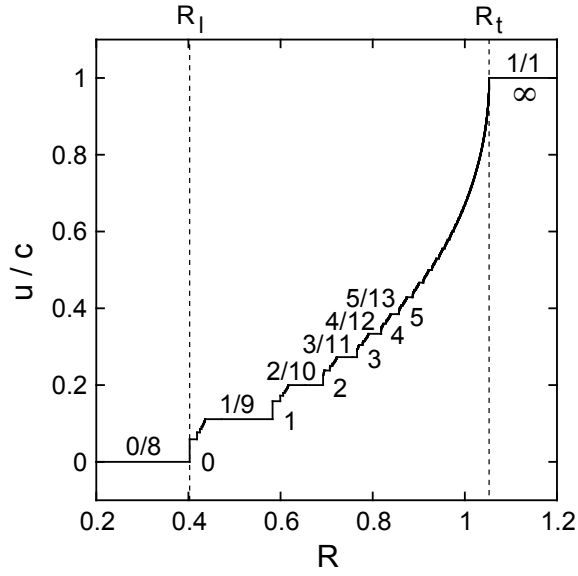


FIG. 6: Average dimensionless particle velocities u/c for the 1D stationary-electrode model with $N = 8$ electrodes per wavelength vs. the dimensionless mobility R , with interior labeling similar to Fig. 5, and with salient features given by the $0/8 \rightarrow 1/1$ Farey sequence. Shown are localization and trapping thresholds $R_l = (1 + \sqrt{2}/2)^{1/2}\pi^2/32 = 0.40$ and $R_t = (1 + \sqrt{2}/2)\pi^2/16 = 1.05$ from Eqs. (16) and (18).

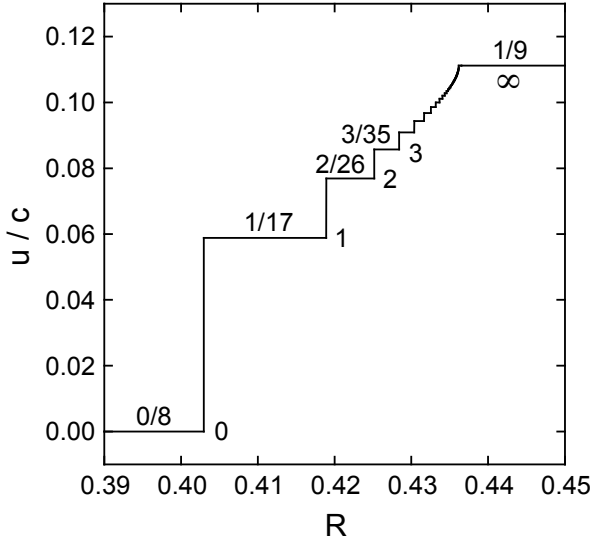


FIG. 7: Detail from Fig. 6 for the $0/8 \rightarrow 1/9$ Farey sequence.

containing an infinite number of sub-sub-steps and so on, Fig. 6 qualifies as a particularly devilish Devil's staircase.

Devil's staircases have zero derivative almost everywhere, and yet the function's value increases through an infinite sequence of steps. Such staircases result when an oscillator locks onto an infinity of driving frequencies [9], and are seen in a variety of physical systems [10–12].

Solutions for $N > 8$ yield even greater complexity, including many levels of nested, overlapping, and bidirec-

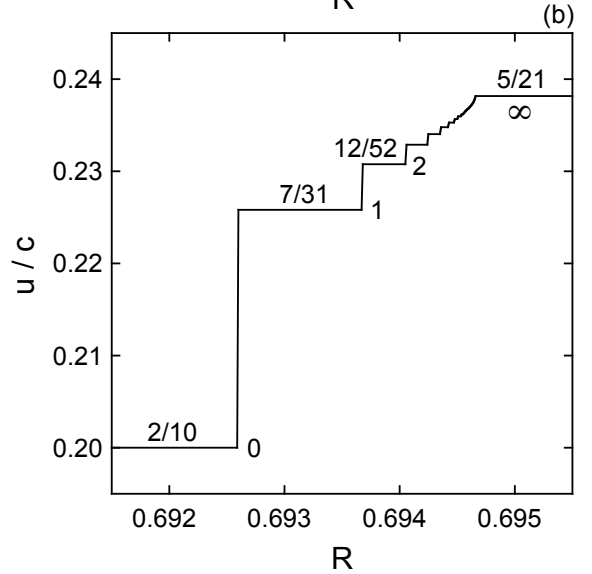
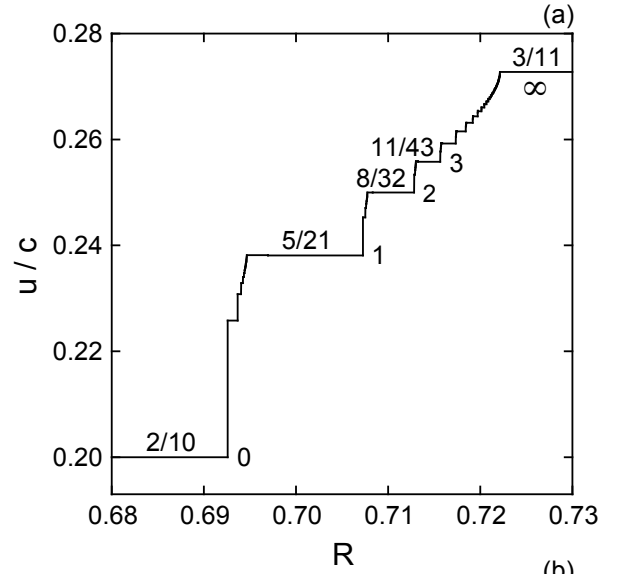


FIG. 8: Detail from Fig. 6 for the $2/10 \rightarrow 3/11$ (a) and $2/10 \rightarrow 5/21$ (b) Farey sequences.

tional Farey sequences. For general N , the main Farey sequence is $0/N \rightarrow 1/1$, which can be represented in plots like Fig. 4 by noting that $t' = N$ is the dimensionless period and $x' = N$ is the dimensionless wavelength. The larger the number N of electrodes per wavelength, the smaller the displacement between electrodes and the smaller the velocity steps in the main Farey sequence. Figure 10 shows how results for increasing N approach the 1D sinusoidal result given by Eq. (4), and include the $N = 3$ case studied earlier [13]. The Shannon-Nyquist theorem [14, 15] demands $N > 2$ for effective transport, in agreement with experiments [16]. The solution for $N = 128$ is indistinguishable graphically from Eq. (4) for the sinusoidal model. This is a fascinating example of an incredibly complex discrete model reducing to simplicity itself when taken to the continuum limit.

Localization and trapping thresholds decrease with in-

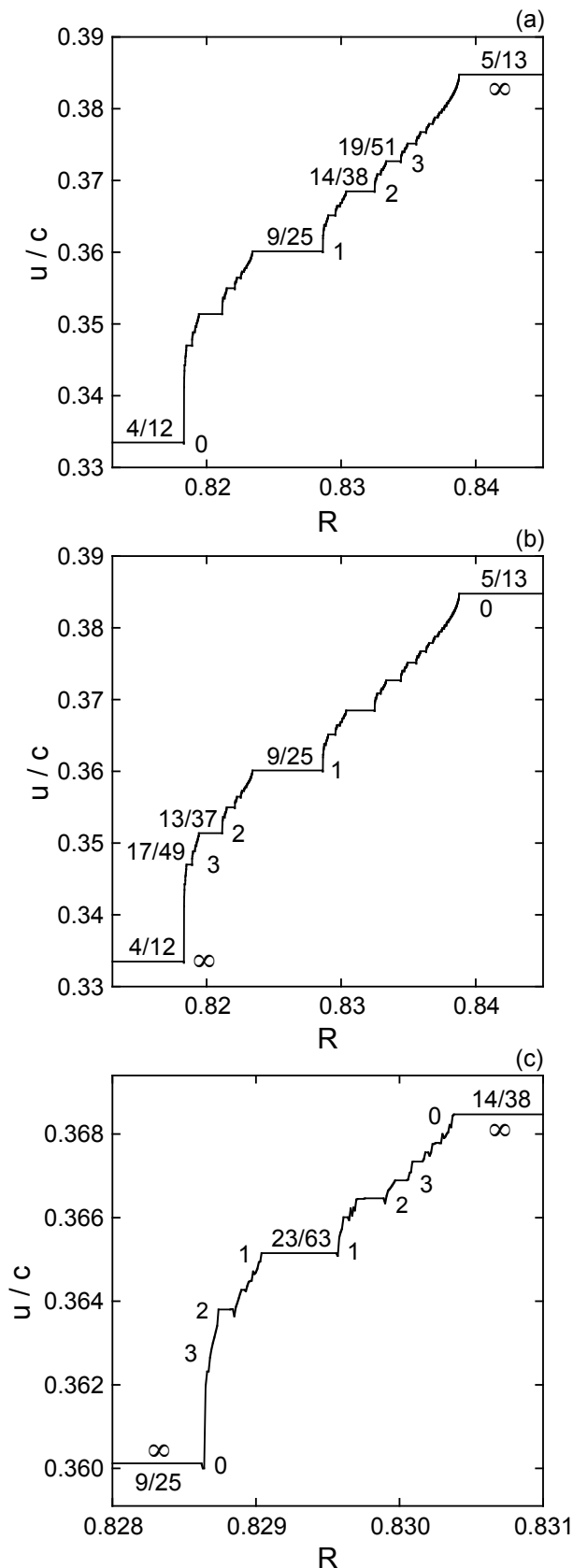


FIG. 9: Detail from Fig. 6 for the $4/12 \rightleftharpoons 5/13$ (a,b) and $9/25 \rightleftharpoons 14/38$ (c) Farey sequences.

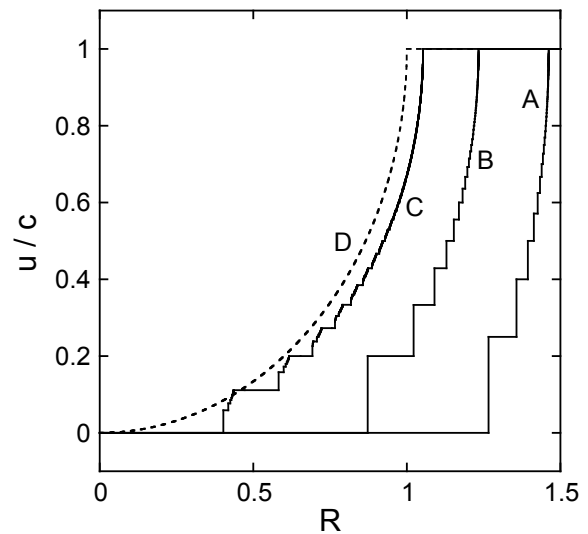


FIG. 10: Average dimensionless particle velocities u/c for the 1D stationary-electrode model with $N = 3, 4$, and 8 electrodes per wavelength (solid traces A, B, and C, respectively) and for the 1D sinusoidal model [dotted trace, D, Eq. (4)], vs. the dimensionless mobility R .

creasing N [See Fig. 10 and Eqs. (16) and (18)] because the ability of a particle to make net forward progress is directly dependent on its ability to reach the next electrode before that electrode loses stability. Fewer electrodes per wavelength translate to a greater distance between electrodes for the same wavelength, and a larger mobility required to travel the distance between two electrodes in the allotted time.

Model differences follow partially from differences in phase-space dimensionalities. In the 1D sinusoidal and traveling-electrode models, the time dependence of the electric field can be eliminated by the simple substitution

$$y = x - ct, \quad (25)$$

reducing the dependence to the single variable y . Any such system has a one-dimensional phase space and will either diverge or be attracted to fixed points; no more complicated behavior is allowed [17]. No such substitution can be made for the 1D stationary-electrode model, whose two-dimensional phase space (depending on x and t) accounts for its stepped behavior but disallows chaos [18]. Models with two spatial dimensions, x and y , and one time dimension t have a three-dimensional phase space and exhibit chaos [2].

IV. CONCLUSIONS

In summary, a 1D stationary-electrode model bridges simple 1D continuum models and more complicated 2D models, uncovers the origin of stepped behaviors, and exhibits rich structure. The 1D sinusoidal and traveling-electrode models lack localization thresholds and velocity

plateaus, both of which are seen in the 2D model. The 1D traveling-electrode model reveals longitudinal oscillations to be the result of consecutive failed attempts by particles to catch a passing wave. The 1D stationary-electrode model features velocity plateaus and mode locking, admits localization and trapping thresholds that can be calculated explicitly, and exhibits many levels of nested, overlapping, and bidirectional Farey sequences and devil's staircases.

Molecular diffusion might complicate the observation of velocity plateaus by smoothing the plot of velocity versus mobility, especially for experiments with fluorescent tracer ions. For this reason, experiments using small concentrations of charged fluorescent beads or quantum dots imaged with confocal microscopy would be particularly welcome. Models that include the role of molecular diffusion and electrode polarization are needed in order to assess their effects on the velocity. Initial studies of the role of molecular diffusion are underway.

V. ACKNOWLEDGMENTS

We gratefully acknowledge support from NSF Grants CBET-1066730 and EPS-0554328, the WV EPSCoR Office, and the WVU Research Corporation.

-
- [1] E. Verpoorte, *Electrophoresis* **23**, 677 (2002).
- [2] B. F. Edwards, *Phys. Rev. E* **80**, 036205 (2009).
- [3] B. F. Edwards, A. T. Timperman, R. L. Carroll, K. D. Jo, J. M. Mease, and J. E. Schiffbauer, *Phys. Rev. Lett.* **102**, 076103 (2009).
- [4] B. R. Reschke, J. E. Schiffbauer, B. F. Edwards, and A. T. Timperman, *Analyst* **135**, 1351-1359 (2010).
- [5] K. D. Jo, J. E. Schiffbauer, B. F. Edwards, R. L. Carroll, and A. T. Timperman, *Analyst* **137**, 875-883 (2012).
- [6] J. R. Melcher, E. P. Warren, and R. H. Kotwal, *Part. Sci. Tech.* **7**, 1-21 (1989).
- [7] H.-H. Wei, *Appl. Phys. Lett.* **90**, 204103 (2007).
- [8] J. Maselko, H. L. Swinney, *J. Chem. Phys.* **85**, pp. 6430-6441 (1986).
- [9] P. Bak, *Physics Today* **39**, pp. 39-45 (1986).
- [10] A. Pikovsky, M. Rosenblum, J. Kurths. *Synchronization: a universal concept in nonlinear sciences* (Cambridge University Press, Cambridge, 2001).
- [11] C. Reichhardt and F. Nori, *Phys. Rev. Lett.* **82**, 414 (1999).
- [12] J. Herrmann, M. Karweit, and G. Drazer, *Phys. Rev. E* **79**, 061404 (2009).
- [13] S. Masuda, M. Washizu, M. Iwadare, *IEEE Trans. Ind. Appl.* **IA-23**, pp. 474-480 (1987).
- [14] C. E. Shannon, *Proc. IRE* **37**, 10 (1949): reprint as classic paper in *Proc. IEEE* **86**, 447 (1998).
- [15] H. Nyquist, *Trans. AIEE* **47**, 617 (1928): reprint as classic paper in *Proc. IEEE* **90**, 280 (2002).
- [16] J. M. Hemstreet, *J. of Electrostatics*, **17**, pp. 245-54 (1985).
- [17] S. H. Strogatz, *Nonlinear Dynamics and Chaos* (Addison-Wesley, New York, 1994), Sec. 2.6
- [18] S. H. Strogatz, *Nonlinear Dynamics and Chaos* (Addison-Wesley, New York, 1994), Sec. 7.3.